

Article

The Advancement and Utilization of Marx Electric Field Generator for Protein Extraction and Inducing Structural Alterations

Voitech Stankevič ^{1,*}, Kamilė Jonynaitė ¹, Ahmed Taha ^{1,2}, Skirmantas Keršulis ¹, Aldas Dervinis ¹, Sebastjanas Kurčevskis ³, Sonata Tolvaišienė ³, Arūnas Stirė ¹ and Nerija Žurauskienė ³

¹ Department of Functional Materials and Electronics, Center for Physical Sciences and Technology, Saulėtekio av. 3, 10257 Vilnius, Lithuania; kamile.jonynaitė@ftmc.lt (K.J.); ahmed.taha@ftmc.lt (A.T.); skirmantas.kersulis@ftmc.lt (S.K.); aldas.dervinis@ftmc.lt (A.D.); arunas.stirke@ftmc.lt (A.S.)

² Department of Food Sciences, Faculty of Agriculture (Saba Basha), Alexandria University, 21531 Alexandria, Egypt

³ Faculty of Electronics, Vilnius Gediminas Technical University (Vilnius TECH), Saulėtekio av. 11, 10223 Vilnius, Lithuania; sebastjanas.kurcevskis@vilniustech.lt (S.K.); sonata.tolvaisiene@vilniustech.lt (S.T.); nerija.zurauskiene@ftmc.lt (N.Ž.)

* Correspondence: voitech.stankevic@ftmc.lt

Abstract: This study introduces an innovative two-range, 12-stage Marx pulse generator employing thyristor switches designed specifically for the electroporation of biological cells. The generator consists of two module capacitors of different capacitances (1 μ F and 0.25 μ F), which enable the generation of electrical pulses with different durations and amplitudes of up to 25 kV. Safety aspects, including overcurrent and overvoltage protection mechanisms, are implemented in both the software and the hardware. In the experimental section, the tests of the Marx generator with resistive load are described in detail, and the results for the voltage fluctuations, pulse duration, and output characteristics of the generator are presented. The advantages of the design, including the high output voltage, the wide range of repetition rates, and the flexibility of the pulse parameters, are emphasized. Additionally, the research showcases the utilization of the devised generator for industrial purposes. Hence, an investigation into the efficiency of protein extraction from microalgae (*Chlorella vulgaris*) and the impacts of pulsed electric fields (PEFs) on the structural characteristics of casein micelles (CSMs) was chosen as an illustrative example. The obtained results provide valuable insights into the application of PEF in food processing and biotechnology and underline the potential of the developed generator for sustainable and environmentally friendly practices.

Keywords: MARX generator; pulsed electric field; microalgal; protein; casein



Citation: Stankevič, V.; Jonynaitė, K.; Taha, A.; Keršulis, S.; Dervinis, A.; Kurčevskis, S.; Tolvaišienė, S.; Stirė, A.; Žurauskienė, N. The Advancement and Utilization of Marx Electric Field Generator for Protein Extraction and Inducing Structural Alterations. *Appl. Sci.* **2024**, *14*, 3886. <https://doi.org/10.3390/app14093886>

Academic Editor: Piotr Gas

Received: 27 March 2024

Revised: 26 April 2024

Accepted: 30 April 2024

Published: 1 May 2024



Copyright: © 2024 by the authors. Licensee MDPI, Basel, Switzerland. This article is an open access article distributed under the terms and conditions of the Creative Commons Attribution (CC BY) license (<https://creativecommons.org/licenses/by/4.0/>).

1. Introduction

The growing interest in sustainability in food processing is leading to the use of various environmentally friendly processing technologies (ultrasound, electric field, etc.) to eliminate the negative impact on the environment and reduce the energy consumption of conventional processing technologies [1]. As an innovative eco-friendly technique, the pulsed electric field (PEF) has been used in various food applications, mainly to deactivate enzymes and microorganisms [2,3]. PEF treatment involves the application of high-voltage electrical pulses to treat food. These pulses are applied between two electrodes for a duration of nanoseconds to milliseconds [4]. Pulse generators play a crucial role in this treatment by converting the long-term input into a short-term output. When developing a pulse generator for the treatment of biological cells, it is important to first determine the required parameters for the generator's output. The selection of these parameters has a significant influence on the biological processes that are triggered in the treated objects. The range of amplitude and duration, repetition frequency, and shape of the electrical

pulses, as well as other parameters of the output pulses, should be selected based on their applicability in these experiments.

Exponential or square pulses are generally used for the electroporation of cells. The use of square pulses is particularly advantageous under laboratory conditions, as they allow the precise control and reproducibility of the relevant electrical parameters, such as pulse length and amplitude [5–8]. However, to generate this pulse shape, capacitors with relatively high capacitance and quite complex switching units should be used. Blumlein or transmission line pulse generators naturally do not have this problem, as the energy is completely discharged during a single pulse [9,10]. However, these generators are limited in terms of maximum voltage and can only generate short pulses of up to one microsecond in duration [5,11]. Exponentially decaying pulse generators with capacitor discharge circuits are widely used due to their simplicity and cost-effectiveness. Various types of these electric field generators have been used in food processing, such as transformer-based generators [12], gas-filled switch-based generators [13], and cascaded solid-state generators [14]. Key features of these generators include the maximum voltage and current amplitude as well as the characteristic time constant (τ), which indicates the time required to reach approximately 37% of the initial potential drop. The Marx generator, which consists of a number (N) of capacitors (C) and switches, is one of these types of generators [15–17]. The advantage of the Marx generator is that a relatively low voltage source is used to generate the high voltage in output. During operation, the capacitors are charged in parallel and then discharged in series via the load (Z_L) by switching on all switches simultaneously. Rise time, fall time, voltage gain (the ratio between the peak value of the output voltage waveform and the input charge voltage of all stages), and full width at half maximum (FWHM) are the defining parameters of an electrical pulse. Depending on the application, the pulses should have certain ranges of the parameters mentioned [18]. The maximum voltage and the maximum current applied to the load Z_L depends on the charging voltage of the capacitors, the number of capacitors, and the internal impedance (Z_{in}) of the device. The width of the electrical pulse also plays an important role. Some studies reported higher inactivation rates when wider pulses were applied [19,20]. On the other hand, Vernhes et al. reported that for pulses of the same specific energy, shorter pulses applied at higher field strengths were more effective in microbial inactivation than wider pulses at lower field strengths [21]. Furthermore, the increased efficiency at longer pulse durations was shown to correlate with the predictions of large cell theory [22]. Since the electroporation of the cell membrane occurs when the induced transmembrane potential exceeds a threshold value (typically about 0.2–1.0 V), the duration of the pulse can in no case be shorter than the minimum time required to reach the transmembrane potential that is specific for the cell type [23]. Therefore, for different applications, for example, protein extraction during microalgae cultivation [24,25] or the change in structural properties of casein micelles [26], various ranges of PEF duration are required. For exponentially decaying pulse generators, the FWHM depends on the time constant, which is calculated according to the equation $\tau = |Z_L + Z_{in}| C/N$. As we can see, one way to control the characteristic time is to change the impedance of the cuvette by changing the resistivity of the liquid or the geometry of the cuvette itself. However, changing the geometry (the distance between the electrodes and the area of the electrodes) has a large effect on the magnitude of the electric field and the current. In addition, we would need to produce different cuvettes to treat different substances. For this reason, the development of an electroporator with the possibility to tune the pulse duration of the switch between different time ranges is of great importance. From another point of view, there are generators that are not only required for processing suspensions in small quantities but also for processing large quantities, especially for industrial applications, for which powerful generators are needed [27,28].

In the present work, we present the development of a Marx pulse generator based on thyristor switches that contain two sets of capacitors with different capacitances and which are capable of generating electrical pulses in two-time ranges. The results of using this generator to study the extraction efficiency of proteins from microalgae (*Chlorella vulgaris*)

and the investigation of the effects of pulsed electric fields on the structural properties of casein micelles (CSMs) are presented.

2. Design of the Generator

2.1. Structure of the Electric Pulse Generator

The block diagram of the Marx generator is shown in Figure 1. In the developed topology of this device, diodes are used for charging capacitors and active semiconductor switches (thyristors) for discharging. Compared to Marx generators that are charged with resistors, diode charging proves to be more efficient as it reduces energy loss by up to 50% compared to charging via resistors [29].

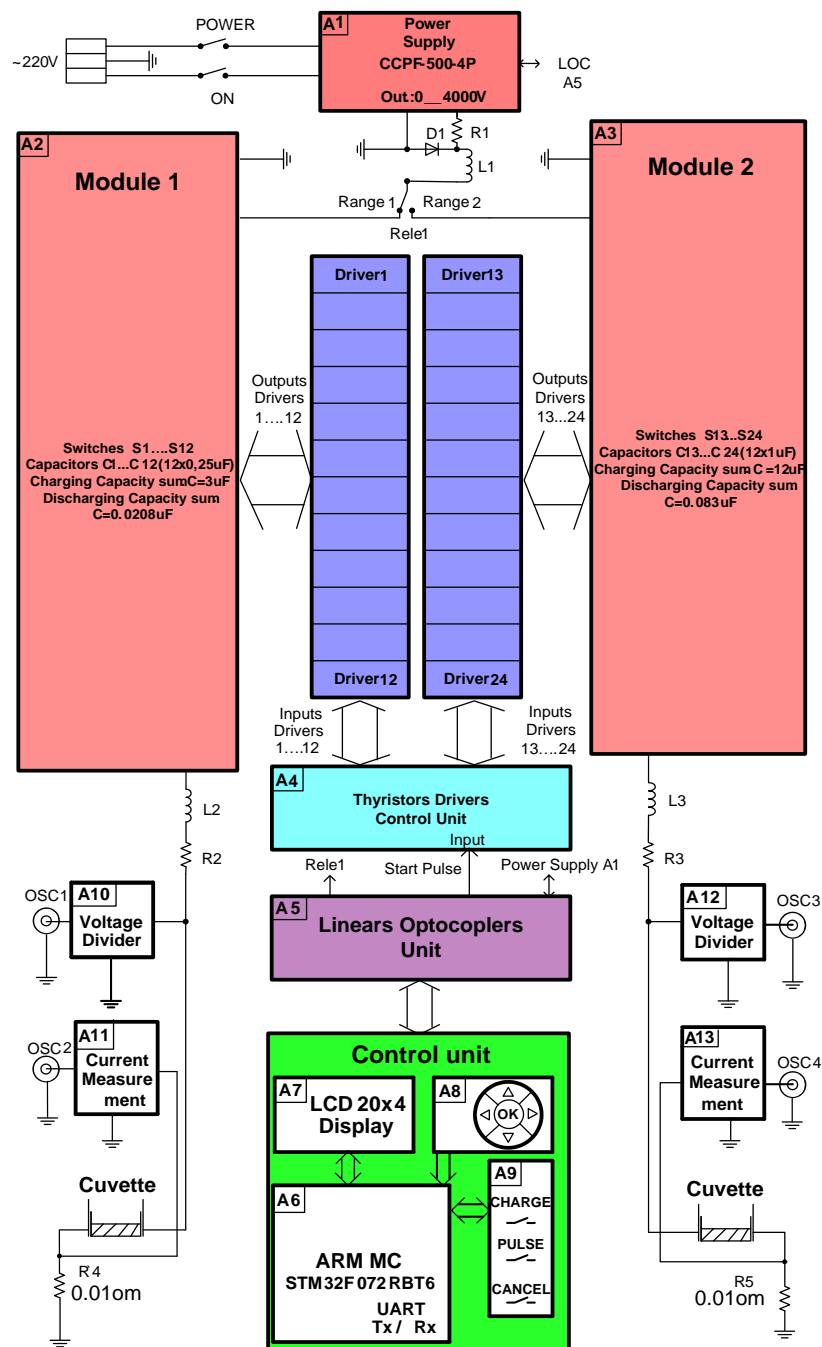


Figure 1. Block diagram of the two-range, 12-stage Marx generator.

The Marx generator, designed to generate electrical pulses with different durations, consists of two modules (A2 and A3) equipped with different capacitors ($C = 0.25 \mu\text{F}$ and $C = 1 \mu\text{F}$). Each module consists of 12 stages, including capacitors, discharge switches (thyristors with drivers), charging diodes, and measuring units for the output voltage (A10 and A12) and current (A11 and A13). Both modules are housed in a common casing, supplied by the same power supply (A1), and controlled by a single control unit.

2.1.1. The High-Power Unit

The variable AC/DC 220/4000 V high-voltage unit, model CCPF-500-4P, Schulz-Electronic GmbH, Baden-Baden, Germany (A1), serves as the supply source (see Figure 1) for both modules. The output voltage of this supply source is controlled by an analog 0–10 V signal from the microcontroller, which corresponds to an output of 0–4 kV. The analog control signal is transmitted via the linear optocoupler unit (A5) and generated in the control unit.

The activation of one of the two modules is controlled by the control unit via a relay, which connects the power supply to the selected module. A more detailed circuit of one of the modules is shown in Figure 2a. The first module consists of twelve $0.25 \mu\text{F}$ (5 kV) polypropylene capacitors, while the second module contains twelve $1 \mu\text{F}$ (5 kV) polypropylene capacitors. These capacitors offer a high repetition rate and a rise time of $11 \text{ kV}/\mu\text{s}$.

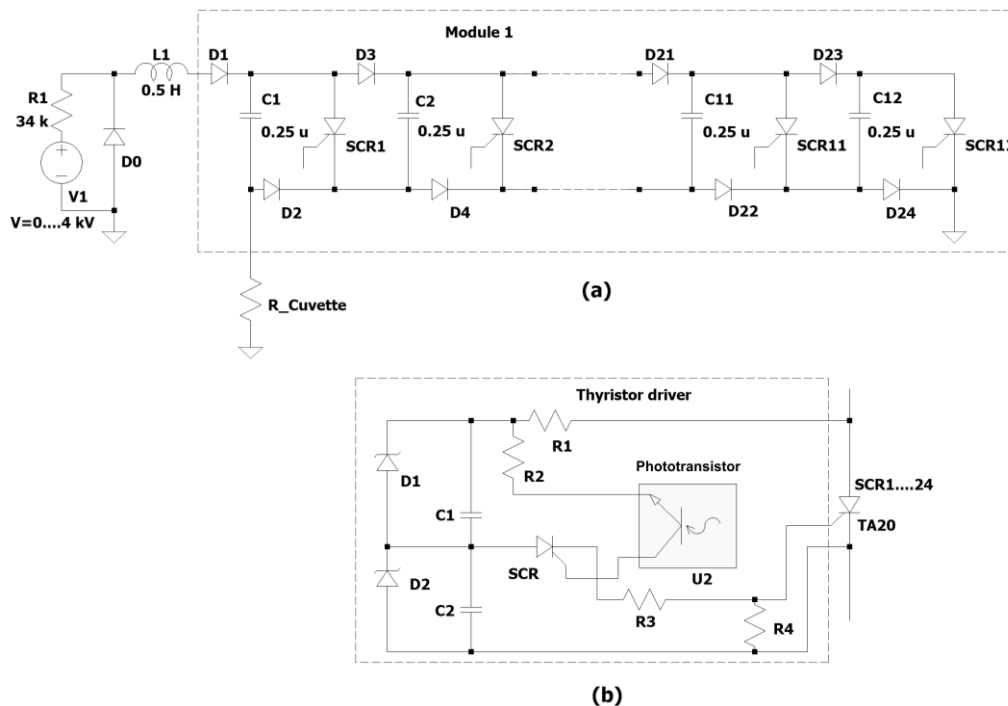


Figure 2. Topology of one of the modules of the Marx generator (a) and thyristor driver (b).

During operation, the capacitors are charged in parallel via diodes (diodes D2–D25 for the module). The capacitors are then discharged by connecting them in series through the load. Thyristors (TA20401203SQ, Powerex Inc., Youngwood, PA USA) with driver modules are used as the switches. These thyristors have a maximum operating voltage of 4000 V and a maximum operating current of 1200 A. Each thyristor is individually controlled by a separate driver, which is controlled by an A4 drive control unit via an optical interface. A more detailed circuit of the thyristor driver is shown in Figure 2b.

Each driver is isolated from the others and is powered by the voltage that drops across the thyristor (between the anode and cathode). The electrical circuit of the drivers generates the pulses required for optimum and simultaneous opening of all thyristors. To protect

the thyristors in the event of a short circuit, resistors R2, R3 and inductances L2, L3 are connected in series with the load. In this scenario, resistors limit the maximum current, while inductances regulate the rate of current rise.

2.1.2. Control and Pulse-Measuring Units

The main component of the control unit is the ARM STM32F072RBT6 (Analog Devices International, Limerick, Ireland) microcontroller (A6 in Figure 1). It controls the charging voltage and the selection of the capacitor module, determines the number and repetition time of the pulses, and measures the voltage on the capacitors. The input parameters of the pulse (voltage, number of pulses, and pulse repetition) are set via the group of five buttons in block A8. All set parameters are shown on the liquid crystal display (LCD) in display A7.

An external oscilloscope is used to visualize the electrical pulse. The voltage value across the load is measured with the voltage dividers A10 and A12, while the current through the load is measured with the non-contact ammeters A11 and A13.

2.2. Operation of the Marx Generator

The operation of the generator can be divided into the following two phases: (1) the input of the pulse parameters and (2) the pulse generation. During the first phase, the microcontroller A6 (see Figure 1) monitors the input and updates the parameters (the module number, charging voltage—up to 3.5 kV—number of pulses—from 1 to 99 or continuous regime—and the pulse repetition period from 1 s) on the LCD screen A7. Entering and exiting this phase is performed by pressing the “OK” button in block A8. Once the main parameters are set, the capacitors can be charged by pressing the “Charge” button in group A9. From this moment on, the system enters the pulse generation phase.

In the pulse generation phase, the microcontroller A6 commands the high voltage power supply A2 via the optical driver A4 to start charging the capacitor connection in block A3. During this process, the voltage of the capacitors is monitored in real-time on the LCD A7. This phase is also indicated by the flashing of the red photodiode until the capacitors are charged to the set voltage. Once the capacitors are charged, pressing the “Pulse” button initiates the discharge of the capacitors via the load.

During this time, the microcontroller sends a command to the control unit of the thyristor drivers and generates optical pulses that are sent to the thyristor drivers. The thyristor drivers form the trigger pulse for the thyristors and open them. The thyristors connect the charged capacitors in series and discharge them via the load. After completion, the system returns to pulse generation and waits for the next command from the user.

2.3. Safety Considerations

The nodes and individual parts of this device are protected against overcurrent and overvoltage. Although the variable high-voltage power supply has internal current limits (250 mA), a resistor $R1 = 5 \text{ k}\Omega$ is connected in series with the capacitors to protect the power supply against the overcurrent. In addition, a diode D1 and an inductor L1 are used to protect the power supply from the negative voltage that can occur when the capacitors are discharged.

To ensure the precise control of the electroporation device, the accurate and safe selection of the pulse parameters for each operating mode is crucial. Therefore, various restrictions are implemented in both the software design and the hardware. The software limits parameters such as the maximum charging voltage, the number of pulses, and the pulse repetition time.

To avoid voltage dips during relay switching, the operation of the relay is synchronized with the high-voltage supply. A separate interruption event is integrated into the software to anticipate a change in the operating module that leads to the high-voltage source being switched off. When the user changes the operating module, the power supply is deactivated, and after confirmation of its status, the relay is switched. This implementation ensures safe commutation of the capacitors and prevents voltage dips during mode selection.

In addition, charged high-voltage capacitors are a potential hazard. If they are switched off for any reason after charging, they can retain a lethal charge over a long period of time. To eliminate this risk, leakage resistors ($10\text{ M}\Omega$ resistors connected to the capacitors) are installed at the terminals to ensure a constant discharge even when disconnected from the pulse circuit. In addition, the device has a forced discharge of the capacitors, which is activated by the “Cancel” button and directs the discharge through the intended circuit.

In addition, ballast resistors (R_2 , R_3) of $5\ \Omega$ and an induction coil (L_2 , L_3) of $5\ \mu\text{H}$ are connected in series with the cuvette to limit the current flow through the thyristors and to control the rise time of the current in the event of an electrical short circuit in the cuvette.

2.4. Design of the Device

A photo of the developed electroporation system can be seen in Figure 3. The developed generator is housed in a metal casing with the dimensions $1.2 \times 0.5 \times 0.5\text{ m}^3$. For ease of use, the front of the device is visually divided into three sections that correspond to the three phases of device operation: parameter input (center), pulse generation (left), and pulse parameter measurement, which is facilitated by a BNC connector for an external oscilloscope, along with a “cancel” button for forced capacitor discharge (right). Pulse parameters are entered into the system via a set of five buttons and an LCD on the left-hand side of the device.



Figure 3. A photo of the developed two-range, 12-stage Marx generator. The oscilloscope is used to measure voltage and current pulses.

Pulses are generated using the two buttons “Charge” and “Pulse” on the left-hand side of the device. This step is also highlighted by the red photodiode. A high-voltage output cable for the load (cuvette with treated substance) is located on the back of the device.

3. Testing of Marx Generator

The Marx generator was tested using a resistive load. First, a single stage of the generator was examined. Figure 4a shows the output voltage across the 50Ω load when the capacitor of capacitance $0.1 \mu\text{F}$ is charged to 300 V . The resistance of the load is characteristic of the cuvettes (VWR International, Taiwan) with buffer liquid used in biological experiments. The trigger pulse formed with a thyristor driver is also shown in the inset of this figure. According to the datasheet for this type of thyristor, the gate trigger current should be higher than 300 mA , and the chosen design of the thyristor driver fully meets this requirement.

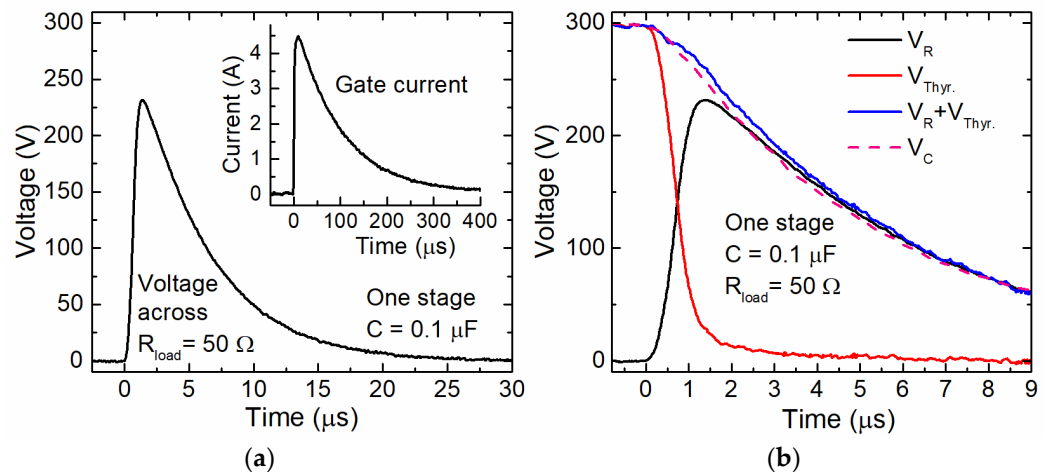


Figure 4. The general shape of the output voltage across the 50Ω load of one stage of the Marx generator (a). The gate current of the thyristor is shown in the inset. Waveforms of the voltage across the thyristor $V_{\text{Thyr.}}$, the load V_R , the capacitor V_C , and the sum voltage of V_R and $V_{\text{Thyr.}}$ (b).

As for the voltage drops across the load, it is clear that the maximum load voltage (about 230 V) is lower than the charged voltage of the capacitor. To understand the reason for this discrepancy, voltage measurements were made across both the capacitor and the thyristor (see Figure 4b). It was found that the switching time of the thyristor was about $1 \mu\text{s}$, and during this time, the voltage was divided between the load and the thyristor. The voltage across the load becomes equal to the voltage across the capacitor only when the thyristor is fully open. However, the capacitor is partially discharged at this point, and the maximum voltage across the load is lower. This is confirmed by the graph, showing the result of summing the voltage across the load and the thyristor (see Figure 4b). As can be seen, the summed voltage is the same as the voltage across the capacitor. Therefore, we can conclude that the lower maximum voltage at the load is not so much caused by the inductance of the circuit, which could also lower the maximum voltage but rather by the opening rate of the thyristor. It should be noted that the use of capacitors with higher capacitance or with higher load resistance reduces this effect due to the slower discharge of the capacitor.

Figure 5 presents the output voltage (V_{out}) across the active load of 416Ω for the 12-stage Marx generator at different charging voltages. Such a load was chosen to become as close as possible to the impedance of the test cell suspension used in electroporation experiments with milk casein (see Section 4.2). As can be seen from this figure, charging the capacitors up to 1.2 kV using a module with a capacitance of $0.25 \mu\text{F}$ (module 1) generated a peak voltage of about 10 kV with a pulse duration at 37% of maximal amplitude at about $14 \mu\text{s}$. When using the second module with a capacitance of $1 \mu\text{F}$, a peak voltage of around 12.5 kV with a half amplitude pulse duration of around $47 \mu\text{s}$ was generated. However, it should be noted that the internal impedance of the generator consisted not only of the reactance of the capacitors but also has an inductive component caused by the wires connecting the thyristors and capacitors. In addition, we also considered the contribution

of inductor coils (L2 and L3) and resistors (R2 and R3) connected in series with the load, which served to reduce the effects of a short circuit in the load. In this case, the maximum voltage and the pulse duration could be different.

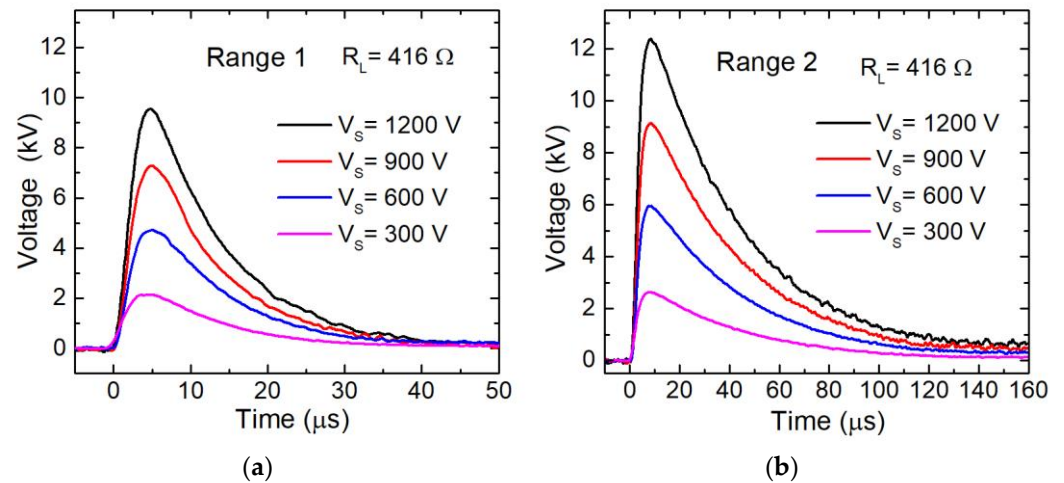


Figure 5. Typical waveforms of the output voltage across the 416 Ω load of the 12-stage Marx generator. (a)—output voltage of the first module (Range 1); (b)—output voltage of the second module (Range 2).

The main advantages of this design are a high output voltage, a wide range of repetition rates, and two ranges of pulse duration.

4. Utilizing the Marx Generator in Biomass Processing

PEF is a versatile tool with myriad applications, particularly in biotechnology. For example, continuous protein extraction or “milking” during microalgae cultivation via PEF treatment is one such application. Microalgae-based products are economical and environmentally friendly as they require little fertile land and freshwater for cultivation [30]. Unlike conventional plants, microalgae thrive in wastewater and reduce pollution by absorbing residual nutrients [31]. Their accelerated reproductive cycle and ability to synthesize a wide range of valuable compounds lead to higher yields over a shorter time span. These unique properties make microalgae a versatile resource for various industrial sectors, including food and feed, pharmaceuticals, and sustainable energy [32].

Another application of PEF is the treatment of proteins with a pulsed electric field that induces a change in the structure of these proteins and their properties. One such type of protein is milk casein. Casein, a milk-derived protein, not only provides essential amino acids and bioactive peptides but is also characterized by its remarkable surface activity, emulsifying properties, self-assembling nature, and unique binding capabilities [33]. These properties make casein micelles a promising source for application in the food and nutraceutical industries. The structures and technical functionalities of casein micelles can be modified by various intrinsic and extrinsic factors. In addition, casein-based products are both economical and environmentally friendly as they efficiently utilize dairy by-products, minimize waste, and optimize the use of resources [34].

For this reason, two substances were selected as examples for the application of a specific electroporator, i.e., Marx generator, namely microalgae and casein.

4.1. Application of the Marx Generator for PEF Treatment of Microalgal Biomass

As mentioned before, one of the applications of the manufactured generator is the electroporation of microalgae. In this Section, we present the results of the treatment of microalgal biomass by electrical pulses.

4.1.1. Materials and Methods of Algal Treatment

The cells of *C. vulgaris* (UTEX 395, Arizona State University) were cultured in a BG-11 medium. The stationary-stage algal culture was used to inoculate the glass bubble column photobioreactor (PBR) (final optical density 0.1 at 750 nm), which was a 1000 mL glass vessel (61 cm in length and 5 cm in diameter) with a downstream aeration tube. The algal suspension was cultured at 22 ± 1 °C with fluorescent lamps at a photosynthetic photon flux density of $90 \mu\text{mol}/\text{m}^2/\text{s}$, a 16:8 h light/dark cycle with a supply of CO_2 and an air-gas mixture until it was harvested at the stationary growth phase (7 days).

Before PEF treatment, the algal suspension was concentrated by centrifugation ($3000 \times g$, 15 min) at a final concentration of 5 g/L, which was determined using optical density (OD) at 750 nm versus a dry biomass calibration curve ($R^2 = 0.962$). The final electrical conductivity and pH of the concentrated suspension were determined using a conductivity meter with InLab 738-ISM probe (Mettler Toledo, Columbus, OH, USA) and Orion 720Aplus (Thermo Scientific™, JAV, Waltham, MA, USA), which were in the range of 2 mS/cm, pH ~7.3.

The algae suspension obtained was processed at room temperature using both modules of the generator described above. The capacitors of the modules were charged from 250 V to 2500 V. A two-electrode electroporation cuvette filled with algae suspension with spacing at $d = 2$ mm (VWR International, Taiwan) was used as the load of the generator. The applied voltage and pulse duration were estimated with the oscilloscope. After PEF treatment, cell permeability, and quantitative and qualitative protein characteristics were evaluated. As a positive control, representing a fully disrupted cell population, the cell suspension was disrupted using the Vibra Cell ultrasonicator (Sonics & Materials Inc., USA) [35].

The permeability of the algal cell membrane after PEF treatment was determined using the dye SYTOX Green (Thermo Fisher Scientific, Newtown, CT, USA). Normally, it is a dye that is impermeable to intact cells. Only after the loss of membrane integrity can SYTOX Green enter the cell, bind to the nucleic acid, and emit fluorescence. In brief, after incubation at room temperature for 2 and 24 h, the treated and untreated samples were diluted to OD 1 (at 750 nm wavelength) with a sterile BG-11 medium. Immediately after dilution, each sample was mixed with a fluorescent dye (final concentration 2 μM) and incubated for 5 min in the dark. The fluorescence intensity was then determined using the LS-50B luminescence spectrometer (PerkinElmer Inc., Buckinghamshire, UK) (excitation at 490 nm, emission at 500–550 nm, peak intensity at 525 nm, scan speed 200 nm/min). To detect the leakage of nucleic acid into the supernatant, SYTOX green fluorescence was also measured in the supernatant after an additional centrifugation step ($6000 \times g$, 1 min).

The concentration of soluble protein in the sample supernatant after 24 h of incubation was determined using the ROTI Quant Universal Assay (Roth, Germany) according to the manufacturer's protocol. The supernatant obtained after centrifugation was also analyzed by SDS-PAGE on a TV200Y electrophoresis instrument (Scie-Plas Ltd., Cambridge, UK) following the modified protocol described in [36,37].

4.1.2. Microalgae Cell Responses to PEF Treatment

To assess the effect of electrical pulses on microalgae, we first determined the duration and voltage of the pulses generated for an algae suspension with a conductivity of $\sigma = 2$ mS/cm and a resistance of $R = 50 \Omega$. Single pulses with a duration of Δt at about 4 μs and 11 μs were generated using the 1st and 2nd range of the generator, respectively. The pulse duration was calculated at the level of 37% of the maximum amplitude. The maximum charging voltages of the capacitor reached 2500 V and 2000 V for ranges 1 and 2, respectively. The characteristic voltage pulses at the cuvette and the current through the cuvette for two ranges of the generator are shown in Figure 6.

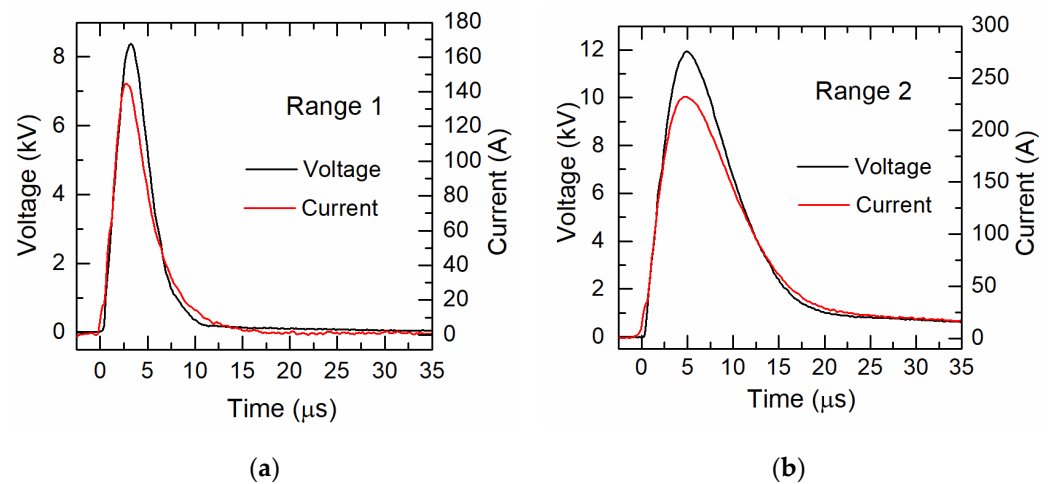


Figure 6. Typical waveforms of the output voltage across the cuvette with microalgae solution (cuvette resistance about 50 Ω). (a)—Output voltage when the cuvette is connected to the first module (Range 1); (b)—when connected to the second module (Range 2).

The electric field in the cuvette was calculated according to the equation $E = V_{\text{out(max)}}/d$, using the peak value of $V_{\text{out(max)}}$. The specific energy W was determined by integrating the voltage and current pulses, taking into account the mass of the suspension. The rise in temperature was also calculated using the adiabatic model. These data are listed in Table 1. Voltages above these thresholds led to sparking in the cuvette.

Table 1. PEF parameters applied to *C. vulgaris* processing.

Range 1 (Pulse Length ~4 μs)			Range 2 (Pulse Length ~11 μs)		
E (kV/cm)	W (J/mL)	ΔT (K)	E (kV/cm)	W (J/mL)	ΔT (K)
2.8	0.05	0.01	4	0.21	0.05
6.35	0.25	0.06	10	1.34	0.32
10	0.61	0.14	16	3.43	0.82
14.8	1.33	0.32	23	7.08	1.69
19.8	2.39	0.57	29	11.26	2.68
25.6	3.99	0.95	34	15.48	3.69
30.8	5.77	1.37	41	22.51	5.36
34.8	7.37	1.76	47	29.58	7.04
46	12.88	3.07			
48.8	14.5	3.45			

The effect of the generated electric field on microalgae was further investigated. To minimize the effects of reversible electroporation, cell permeability measurements were performed at 2 and 24 h after PEF treatment (Figure 7). In addition, indirect effects, such as the leakage of DNA and soluble proteins from the cells, were investigated in PEF-treated and untreated samples.

The data obtained showed that the application of a 4 μs pulse (Range 1) induced an increase in the SYTOX green fluorescence signal only when the applied E exceeded 20 kV/cm or W reached 2.39 J/mL (Figure 7a). In contrast, a lower E of 16 kV/cm and W of 3.43 J/mL were required to induce cell permeability in the second range (with a pulse duration of 11 μs) (Figure 7b). During the following day, the SYTOX signal increased even more in the samples exposed to electric field strengths above the threshold. In addition to the increased permeability of the algal membrane, the leakage of nucleic acids into the supernatant was also observed, with the intensity being highest after prolonged incubation (24 h after PEF). The observed leakage of nucleic acids is a hallmark of programmed cell death, which is a process known to be triggered in *C. vulgaris* by the PEF-induced release of a cell death factor that was recently described here [38]. Their studies showed that

programmed cell death occurs independently of PEF treatment with low or high energy (when $1 \mu\text{s}$, 40 kV/cm pulses are used). Furthermore, they identified cell debris rich in cell death-inducing factors that could lead to death in intact/untreated algae [38]. Although the origin of this compound remains unclear, Canelli et al. identified several *C. vulgaris* protein compounds are involved in the hydrolysis of structures associated with the algal cell wall [39].

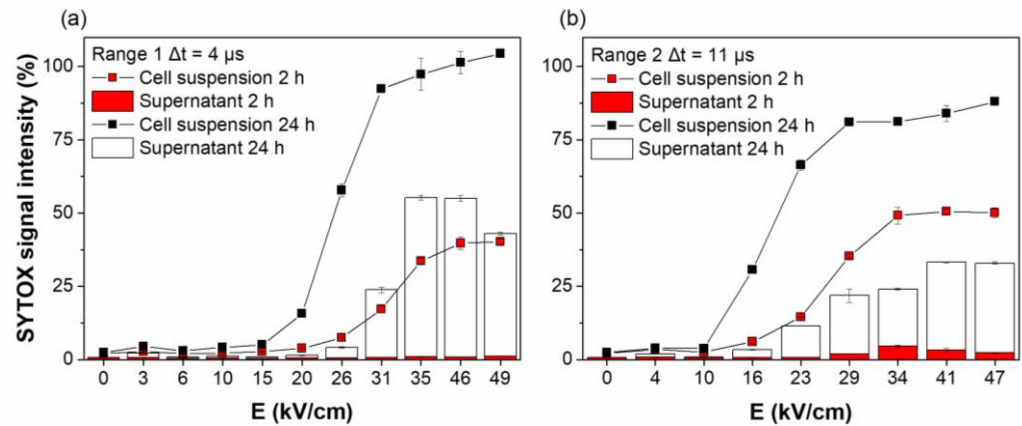


Figure 7. SYTOX green fluorescence in microalgae suspension and supernatant after PEF treatment using Range 1 (a) and Range 2 (b) of the electroporator under different electric field strengths 2 or 24 h post-treatment.

In addition to PEF-induced cell damage and cell death, one of the most valuable compounds—protein release—was also determined in this study (see Figure 8). The results showed that protein release only occurred when the integrity of the algal cell membrane was compromised, which is consistent with the threshold values observed in membrane permeabilization experiments. For shorter pulses (range 1), the threshold for protein release was 20 kV/cm . For longer pulses (range 2), however, this threshold was already triggered at an electric field strength of 16 kV/cm . It should be also noted that even at the maximum applied voltage, the temperature of the suspension did not rise by more than 7 degrees (see Table 1). However, further increases in electric field strength did not affect the increase in protein extraction efficiency, which reached a saturation level for water-soluble proteins.

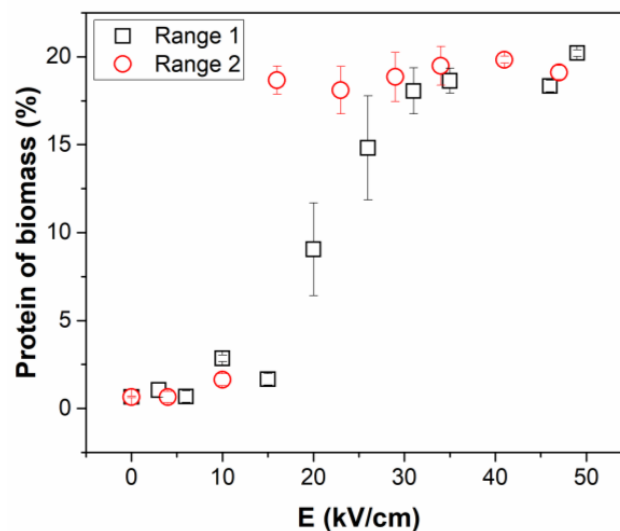


Figure 8. Extracted protein concentration of *C. vulgaris* after treatment with different electric field strengths and operation ranges.

Similar results of PEF-extracted protein yield and its saturation phenomena have been observed in previous studies, suggesting that PEFs induce soluble protein release, which is closely linked to active biological processes, such as the release of factors that trigger programmed cell death. This link proceeds beyond the solely physical phenomena of pore formation [25,38]. However, it is important to note that the parameters of the PEFs used were different in the various studies, although they produced the same effect. Likely reasons for these differences are variations in cultivation and extraction conditions. These include not only the chemical composition of the medium (TAP instead of BG-11) and physical differences (electrical conductivity, pH) but also the scale of cultivation (Erlenmeyer flask instead of a bubble bioreactor). These factors influence not only the cell size and wall composition of the *C. vulgaris* cells but also the efficiency of protein synthesis [40].

The validity of the PEF-induced protein extraction and its quantitative analysis was confirmed using the SDS-PAGE gel images (Figure 9). The gels clearly showed that protein extraction only occurred when the applied electric field (E) exceeded the selectively determined threshold. In particular, the most noticeable protein fractions were obtained in the 1st range at an E above 30 kV/cm, while the threshold value for the 2nd range was 20 kV/cm. However, no distinct protein fractions were observed at $E = 20$ kV/cm and 26 kV/cm for the 1st range and 16 kV/cm for the 2nd range despite the effect on the algae shown in the permeabilization results (Figures 8 and 9). The observed inconsistency was probably due to the much smaller scale of biological processes triggered when PEF was applied in the threshold region. Therefore, the release of water-soluble proteins, which is an enzymatically driven process, requires a longer period to produce a comparable amount of protein, as observed at a higher E [25].

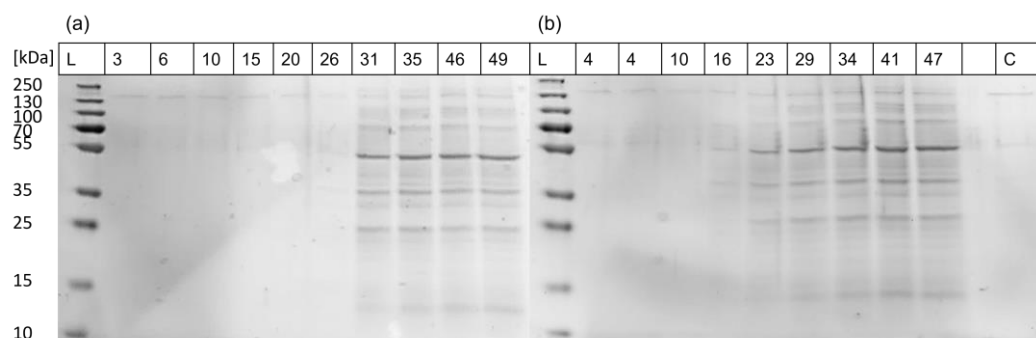


Figure 9. Visualization of PEF-extracted proteins by SDS-PAGE analysis. The numbers above the gels indicate the strength of the applied electric field (in kV/cm) in Range 1 (a) and Range 2 (b). ‘L’ denotes the ladder, and ‘C’ indicates the control.

Moreover, a further increase in E did not lead to the release of additional proteins. The profiles of these fractionated proteins remained consistent across all lanes, with prominent bands at 55, 35, 25, and 15 kDa. These profiles are consistent with known protein fractions obtained after the PEF treatment of *C. vulgaris*, with specific bands associated with proteins, such as ribulose-1,5-bisphosphate carboxylase/oxygenase (RuBisCo, found in the chloroplast), cytochrome c oxidase subunit II (COXII, found in mitochondria), histone H3 (found in the nucleus), and actin (filaments in the cytosol) [25].

4.2. Application of the Marx Generator for PEF Treatment of Milk Casein

Another possible application of the developed Marx generator is the treatment of milk casein. In this Section, the results of the treatment of casein micelles using flow-cuvette and applying strong electrical pulses are presented and discussed.

4.2.1. Materials and Methods of CSM Treatment

The generator produced was also used to process milk casein in a pulsed electric field. Casein micelles (CSM, 92% protein) were purchased from VWR Chemicals (Leuven,

Belgium). Sodium hydroxide and sodium chloride were obtained from AppliChem GmbH (Darmstadt, Germany).

CSM protein suspension (1%, *w/v*) was prepared in potassium phosphate buffer (0.1 M, pH = 7) and stirred overnight. The protein suspension with an electrical conductivity of about 1.4 mS/cm was then treated using both ranges of the Marx generator when the capacitors were charged to 500–1500 V. For this treatment, a modular serial flow-through co-linear chamber was designed with two active treatment areas and the meshes in contact with the electrodes. The design of this chamber was the same as the chamber described in ref. [41]. The stainless steel meshes in this chamber act as electrodes and provide a homogeneous distribution of the electric field in the active treatment areas. The distance between these meshes was 5 mm when the diameter of the treatment region was about 15 mm. The average resistance of the chamber with this suspension was about 400 Ω .

During the experiment, the suspension was pumped into the tubes using a peristaltic pump (Masterflex, Cole-Parmer, Vernon Hills, IL, USA). The flow rate was adapted to the repetition frequency of the generator pulses so that each “portion” of the suspension (located between the electrodes and affected by the electric field) was treated with only one pulse. This made it possible to obtain more correct results. The characteristic repetition of electrical impulses in this case was 1 Hz. Such a time interval between pulses was sufficient to fully load the capacitors. The repetition rate as well as the shape of the pulses, and the maximum voltage were stable. To avoid turbulence processes in the liquid in the cuvette caused by the electrode grid and the change in the shape of the channel in the cuvette, it was also necessary to limit the flow rate of this liquid. Therefore, this limited the maximal repetition rate of the pulse. The electroporation chamber was set up in a vertical position. The voltage pulses at the electrodes, and the current was recorded with an oscilloscope. In these experiments, a protein suspension of about 50 mL was treated.

The particle size and ζ -potential were measured using the dynamic laser light scattering (DLS) of protein samples before and after electroporation using a Malvern Zetasizer analyzer (Nano ZS, Malvern Instrument Co., Ltd., Worcestershire, UK). The diluted samples (1:20) were measured at refractive indexes of 1.45 and 1.33 for the protein and dispersant, respectively [42].

The protein concentration was adjusted to 0.5 mg/mL with 0.1 M phosphate buffer (pH 7.0). In total, 3 mL of each sample was added to a quartz cuvette with a 10 mm path length. The intrinsic fluorescence spectra were recorded with an LS-50B luminescence spectrometer (PerkinElmer Inc., UK). The excitation and emission slit were 10 nm. The fluorescence emission spectra were recorded from 300 to 450 nm at an excitation wavelength of 290 nm [43].

All experiments were performed in triplicate. Mean values and standard deviations were calculated. The results were analyzed by one-way analysis of variance (ANOVA) using Excel software and SPSS (IBM SPSS Statistics, Version 25, SPSS Inc., Chicago, IL, USA) with a statistical significance of $p < 0.05$.

4.2.2. Particle Size and ζ -Potential Analysis

Table 2 shows the effects of PEF treatment generated using a Marx generator (in both ranges) on the particle sizes of CSMs. The particle sizes of protein molecules increased after PEF treatment. This could be probably due to the partial denaturation or aggregation of CSM's globular structure after PEF treatment [44]. Similar results were observed in our recent study [26] in which PEF treatment (10 kV/cm) increased the size of CSMs using another type of PEF generator. The ζ -potential of CSM proteins (Table 2) increased after PEF treatment. There was no significant change in the ζ -potential after PEF treatment. The increase in ζ -potential may increase the electrostatic repulsions, altering the functional properties of proteins [45]. PEF treatment could generate free radicals, increasing the absolute ζ -potential value around protein molecules [4].

Table 2. Particle size parameters (z-average) and ζ -potential protein solubility of PEF-treated and untreated CSM. Means with different letters (a, b, c) within the same column indicate statistically significant differences between the samples after Duncan's analysis ($p < 0.05$).

Samples	Range 1 (Pulse Length $\sim 9 \mu\text{s}$)		Samples	Range 2 (Pulse Length $\sim 25 \mu\text{s}$)	
	Z-Average (nm)	ζ -Potential (mV)		Z-Average (nm)	ζ -Potential (mV)
Control	166.4 \pm 2.1 ^b	−30.5 \pm 2.4 ^a	Control	166.4 \pm 1.5 ^c	−30.5 \pm 1.8 ^a
3 kV/cm	198.0 \pm 3.5 ^a	−35.5 \pm 1.9 ^b	7 kV/cm	175.7 \pm 2.7 ^b	−36.2 \pm 2.4 ^b
8.8 kV/cm	203.3 \pm 2.3 ^a	−36.6 \pm 1.4 ^b	14.8 kV/cm	181.2 \pm 1.8 ^a	−36.7 \pm 3.1 ^b
16 kV/cm	197.8 \pm 1.6 ^a	−36.1 \pm 2.1 ^b	22.6 kV/cm	172.2 \pm 1.4 ^b	−35.8 \pm 2.9 ^b

The changes in the fluorescence spectra of proteins were considered an indicator for the changes in the proteins' tertiary structure induced by the microenvironment polarity changes in the tyrosine (Tyr) and tryptophan (Trp) residues [46,47]. To verify that the alterations in CSM's structure resulted from PEF treatment, Figure 10 illustrates the shifts in fluorescence spectra between untreated and PEF-treated protein samples, revealing a decrease in fluorescence intensity following PEF treatment. This suggests that tryptophan moieties were less exposed to excitation, as lower emission intensities were observed. Tryptophan's fluorescence is reliant on the polarity of its microenvironment. In the tertiary structure, tryptophan residues were buried in nonpolar and hydrophobic regions. After unfolding the protein structure, tryptophan residues were exposed to aqueous polar media, quenching their fluorescence signals. Tryptophan's fluorescence quenching could also be related to the tertiary structure's conformational changes, including the dissolution of hydrophobic interactions and/or the crosslinking of amino acid side chains [44]. In another study, the fluorescence intensity of the PEF-treated (4–10 V/cm) soy protein isolate was higher than the native untreated protein [48]. This could be due to the differences in the nature and structure of proteins and/or the different applied electric field strengths.

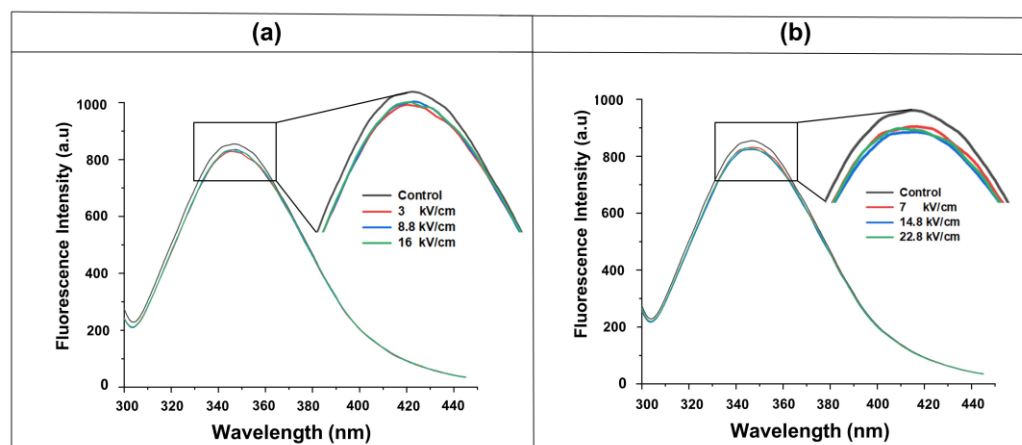


Figure 10. Fluorescence emission spectra of control (0 kV/cm) and PEF-treated casein micelles at different electric field strengths and operation Range 1 (a) and Range 2 (b).

5. Conclusions

In conclusion, this manuscript presents the design and implementation of a two-range Marx pulse generator using thyristor switches for biomass processing. By using diode-based charging and semiconductor switches, the generator achieves higher efficiency compared to traditional Marx generators with resistor-based charging. The installation of two modules with different capacitances of capacitors enables flexibility in the generation of pulses. The control unit, operated by a microcontroller, allows precise parameter adjustment and pulse generation, ensuring user safety and ease of operation.

Moreover, safety considerations integrated into the system's design mitigate potential risks associated with high-voltage capacitors, such as overcurrent and overvoltage protection and the precise control of pulse parameters. The test of the Marx generator confirmed the performance of this device, highlighting its ability to produce high output voltages with adjustable repetition rate and pulse duration, positioning it as a valuable tool in various applications requiring controlled electrical pulses. The application of this generator is demonstrated through the treatment of microalgae (*C. vulgaris*) and casein micelles (CSMs) with pulsed electric fields (PEFs). Microalgae, with their economical and environmentally friendly attributes, showcase increased membrane permeability, nucleic acid leakage, and protein release under PEF treatment. Casein micelles, known for their unique properties, exhibited changes in particle size, ζ -potential, solubility, intrinsic fluorescence, and Fourier transform infrared spectroscopy profiles following PEF treatment.

The presented results emphasize the significance of the generated electric field's strength and duration, demonstrating the threshold conditions for optimal biological effects. The Marx generator's ability to achieve varied pulse parameters enables a nuanced exploration of the impact of PEF on different biological materials. Overall, this work contributes to the field of green processing technologies, providing a reliable and versatile electroporation tool for diverse applications in the food and biotechnology industries. The outcomes from the investigation of microalgae and casein micelles serve as valuable insights into the potential applications and effects of PEF on different biological systems.

Author Contributions: Conceptualization, V.S., A.T. and K.J.; methodology, V.S., K.J., A.T., S.K. (Sebastjanas Kurčevskis), A.S. and N.Ž.; software, S.T., S.K. (Sebastjanas Kurčevskis), S.K. (Skirmantas Keršulis) and A.D.; validation, K.J., A.T., S.K. (Sebastjanas Kurčevskis), S.K. (Skirmantas Keršulis), S.T. and A.S.; formal analysis, V.S., N.Ž., K.J., A.T., A.S. and S.K. (Sebastjanas Kurčevskis); investigation, K.J., A.D., A.T., S.K. (Sebastjanas Kurčevskis) and S.K. (Skirmantas Keršulis); resources, K.J., A.T. and A.S.; data curation, K.J., A.T., A.S. and V.S.; writing—original draft preparation, V.S., K.J., A.S., A.T. and N.Ž.; writing—review and editing, V.S., K.J., N.Ž., A.T. and A.S.; visualization, A.D., S.T., A.T. and V.S.; supervision, V.S. and K.J. All authors have read and agreed to the published version of the manuscript.

Funding: This work was supported by the Research Council of Lithuania under grant P-MIP-22-257.

Institutional Review Board Statement: Not applicable.

Informed Consent Statement: Not applicable.

Data Availability Statement: Data are contained within the article.

Conflicts of Interest: The authors declare no conflicts of interest.

References

1. Režek Jambrak, A.; Nutrizio, M.; Djekić, I.; Pleslić, S.; Chemat, F. Internet of Nonthermal Food Processing Technologies (IoNTP): Food Industry 4.0 and Sustainability. *Appl. Sci.* **2021**, *11*, 686. [[CrossRef](#)]
2. Jaeger, H.; Meneses, N.; Knorr, D. Impact of PEF Treatment Inhomogeneity Such as Electric Field Distribution, Flow Characteristics and Temperature Effects on the Inactivation of *E. coli* and Milk Alkaline Phosphatase. *Innov. Food Sci. Emerg. Technol.* **2009**, *10*, 470–480. [[CrossRef](#)]
3. Alirezalu, K.; Munekata, P.E.S.; Parniakov, O.; Barba, F.J.; Witt, J.; Toepfl, S.; Wiktor, A.; Lorenzo, J.M. Pulsed Electric Field and Mild Heating for Milk Processing: A Review on Recent Advances. *J. Sci. Food Agric.* **2020**, *100*, 16–24. [[CrossRef](#)]
4. Giteru, S.G.; Oey, I.; Ali, M.A. Feasibility of Using Pulsed Electric Fields to Modify Biomacromolecules: A Review. *Trends Food Sci. Technol.* **2018**, *72*, 91–113. [[CrossRef](#)]
5. Reberšek, M.; Miklavčič, D. Advantages and Disadvantages of Different Concepts of Electroporation Pulse Generation. *Automatika* **2011**, *52*, 12–19. [[CrossRef](#)]
6. Stankevič, V.; Simonis, P.; Zurauskiene, N.; Stirke, A.; Dervinis, A.; Bleizgys, V.; Kersulis, S.; Balevicius, S. Compact Square-Wave Pulse Electroporator with Controlled Electroporation Efficiency and Cell Viability. *Symmetry* **2020**, *12*, 412. [[CrossRef](#)]
7. Stankevič, V.; Novickij, V.; Balevicius, S.; Žurauskienė, N.; Baškys, A.; Dervinis, A.; Bleizgys, V. Electroporation System Generating Wide Range Square-Wave Pulses for Biological Applications. In Proceedings of the 2013 IEEE Biomedical Circuits and Systems Conference (BioCAS), Rotterdam, The Netherlands, 31 October–2 November 2013; pp. 33–36.

8. Stirke, A.; Zimkus, A.; Balevicius, S.; Stankevici, V.; Ramanaviciene, A.; Ramanavicius, A.; Zurauskiene, N. Permeabilization of Yeast *Saccharomyces Cerevisiae* Cell Walls Using Nanosecond High Power Electrical Pulses. *Appl. Phys. Lett.* **2014**, *105*, 253701. [[CrossRef](#)]
9. Kolb, J.F.; Kono, S.; Schoenbach, K.H. Nanosecond Pulsed Electric Field Generators for the Study of Subcellular Effects. *Bioelectromagnetics* **2006**, *27*, 172–187. [[CrossRef](#)]
10. Balevičius, S.; Stankevič, V.; Žurauskienė, N.; Shatkovskis, E.; Stirke, A.; Bitinaitė, A.; Saulė, R.; Maciulevičienė, R.; Saulis, G. System for the Nanoporation of Biological Cells Based on an Optically-Triggered High-Voltage Spark-Gap Switch. *IEEE Trans. Plasma Sci.* **2013**, *41*, 2706–2711. [[CrossRef](#)]
11. Beveridge, J.R.; MacGregor, S.J.; Anderson, J.G.; Fouracre, R.A. The Influence of Pulse Duration on the Inactivation of Bacteria Using Monopolar and Bipolar Profile Pulsed Electric Fields. *IEEE Trans. Plasma Sci.* **2005**, *33*, 1287–1293. [[CrossRef](#)]
12. Li, S.; Gao, J.; Sack, M.; Yang, H.; Qian, B.; Mueller, G. Study on a Solid-State Pulse Generator Based on Magnetic Switch for Food Treatments by Pulsed Electric Field (PEF). In Proceedings of the 1st World Congress on Electroporation and Pulsed Electric Fields in Biology, Medicine and Food & Environmental Technologies, Portorož, Slovenia, 6–10 September 2015; Jarm, T., Kramar, P., Eds.; Springer: Singapore, 2016; pp. 55–59.
13. Gad, A.; Jayaram, S.H.; Pritzker, M. Performance of Electrode Materials during Food Processing by Pulsed Electric Fields. In Proceedings of the 2013 Abstracts IEEE International Conference on Plasma Science (ICOPS), San Francisco, CA, USA, 16–21 June 2013; p. 1. [[CrossRef](#)]
14. Krishnaveni, S.; Subhashini, R.; Rajini, V. Inactivation of Bacteria Suspended in Water by Using High Frequency Unipolar Pulse Voltage. *J. Food Process Eng.* **2017**, *40*, e12574. [[CrossRef](#)]
15. Baek, J.W.; Yoo, D.W.; Rim, G.H.; Lai, J.-S. Solid State Marx Generator Using Series-Connected IGBTs. *IEEE Trans. Plasma Sci.* **2005**, *33*, 1198–1204. [[CrossRef](#)]
16. Zhong, Z.; Rao, J.; Liu, H.; Redondo, L.M. Review on Solid-State-Based Marx Generators. *IEEE Trans. Plasma Sci.* **2021**, *49*, 3625–3643. [[CrossRef](#)]
17. Zabihi, S.; Zabihi, Z.; Zare, F. A Solid-State Marx Generator with a Novel Configuration. *IEEE Trans. Plasma Sci.* **2011**, *39*, 1721–1728. [[CrossRef](#)]
18. Zabihi, S.; Zare, F.; Ledwich, G.; Ghosh, A.; Akiyama, H. A New Family of Marx Generators Based on Commutation Circuits. *IEEE Trans. Dielectr. Electr. Insul.* **2011**, *18*, 1181–1188. [[CrossRef](#)]
19. Wouters, P.C.; Dutreux, N.; Smelt, J.P.P.M.; Lelieveld, H.L.M. Effects of Pulsed Electric Fields on Inactivation Kinetics of *Listeria Innocua*. *Appl. Environ. Microbiol.* **1999**, *65*, 5364–5371. [[CrossRef](#)] [[PubMed](#)]
20. Aronsson, K.; Lindgren, M.; Johansson, B.R.; Rönner, U. Inactivation of Microorganisms Using Pulsed Electric Fields: The Influence of Process Parameters on *Escherichia coli*, *Listeria innocua*, *Leuconostoc mesenteroides* and *Saccharomyces cerevisiae*. *Innov. Food Sci. Emerg. Technol.* **2001**, *2*, 41–54. [[CrossRef](#)]
21. Vernhes, M.C.; Benichou, A.; Pernin, P.; Cabanes, P.A.; Teissié, J. Elimination of Free-Living Amoebae in Fresh Water with Pulsed Electric Fields. *Water Res.* **2002**, *36*, 3429–3438. [[CrossRef](#)] [[PubMed](#)]
22. Kotnik, T.; Miklavčič, D.; Slivnik, T. Time Course of Transmembrane Voltage Induced by Time-Varying Electric Fields—A Method for Theoretical Analysis and Its Application. *Bioelectrochem. Bioenerg.* **1998**, *45*, 3–16. [[CrossRef](#)]
23. De Vito, F.; Ferrari, G.; Lebovka, N.I.; Shynkaryk, N.V.; Vorobiev, E. Pulse Duration and Efficiency of Soft Cellular Tissue Disintegration by Pulsed Electric Fields. *Food Bioprocess Technol.* **2008**, *1*, 307–313. [[CrossRef](#)]
24. Postma, P.R.; Pataro, G.; Capitoli, M.; Barbosa, M.J.; Wijffels, R.H.; Eppink, M.H.M.; Olivieri, G.; Ferrari, G. Selective Extraction of Intracellular Components from the Microalga *Chlorella Vulgaris* by Combined Pulsed Electric Field–Temperature Treatment. *Bioresour. Technol.* **2016**, *203*, 80–88. [[CrossRef](#)] [[PubMed](#)]
25. Scherer, D.; Krust, D.; Frey, W.; Mueller, G.; Nick, P.; Gusbeth, C. Pulsed Electric Field (PEF)-Assisted Protein Recovery from *Chlorella Vulgaris* Is Mediated by an Enzymatic Process after Cell Death. *Algal Res.* **2019**, *41*, 101536. [[CrossRef](#)]
26. Taha, A.; Casanova, F.; Šimonis, P.; Stankevič, V.; Gomaa, M.A.E.; Stirke, A. Pulsed Electric Field: Fundamentals and Effects on the Structural and Techno-Functional Properties of Dairy and Plant Proteins. *Foods* **2022**, *11*, 1556. [[CrossRef](#)] [[PubMed](#)]
27. Sack, M. Marx-Generator Design and Development for Biomass Electroporation. In *Handbook of Electroporation*; Miklavčič, D., Ed.; Springer International Publishing: Cham, Switzerland, 2017; pp. 793–812. ISBN 978-3-319-32886-7.
28. Mahnič-Kalamiza, S.; Vorobiev, E.; Miklavčič, D. Electroporation in Food Processing and Biorefinery. *J. Membr. Biol.* **2014**, *247*, 1279–1304. [[CrossRef](#)] [[PubMed](#)]
29. Tatur, V.V. Modification of Marx Generator with a Doubling of Output Voltage. *Int. J. Circuit Theory Appl.* **2015**, *43*, 415–420. [[CrossRef](#)]
30. Rajesh Banu, J.; Preethi; Kavitha, S.; Gunasekaran, M.; Kumar, G. Microalgae Based Biorefinery Promoting Circular Bioeconomy—Techno Economic and Life-Cycle Analysis. *Bioresour. Technol.* **2020**, *302*, 122822. [[CrossRef](#)] [[PubMed](#)]
31. Su, Y. Revisiting Carbon, Nitrogen, and Phosphorus Metabolisms in Microalgae for Wastewater Treatment. *Sci. Total Environ.* **2021**, *762*, 144590. [[CrossRef](#)] [[PubMed](#)]
32. Alam, M.A.; Xu, J.L.; Wang, Z. *Microalgae Biotechnology for Food, Health and High Value Products*; Springer: Singapore, 2020; ISBN 9789811501692.
33. Broyard, C.; Gaucheron, F. Modifications of Structures and Functions of Caseins: A Scientific and Technological Challenge. *Dairy Sci. Technol.* **2015**, *95*, 831–862. [[CrossRef](#)]

34. Sadiq, U.; Gill, H.; Chandrapala, J. Casein Micelles as an Emerging Delivery System for Bioactive Food Components. *Foods* **2021**, *10*, 1965. [[CrossRef](#)]
35. Sommer, M.-C.; Balazinski, M.; Rataj, R.; Wenske, S.; Kolb, J.F.; Zocher, K. Assessment of Phycocyanin Extraction from *Cyanidium Caldarium* by Spark Discharges, Compared to Freeze-Thaw Cycles, Sonication, and Pulsed Electric Fields. *Microorganisms* **2021**, *9*, 1452. [[CrossRef](#)]
36. Laemmli, U.K. Cleavage of Structural Proteins during the Assembly of the Head of Bacteriophage T4. *Nature* **1970**, *227*, 680–685. [[CrossRef](#)] [[PubMed](#)]
37. Coustets, M.; Joubert-Durigneux, V.; Hérault, J.; Schoefs, B.; Blanckaert, V.; Garnier, J.-P.; Teissié, J. Optimization of Protein Electroextraction from Microalgae by a Flow Process. *Bioelectrochemistry* **2015**, *103*, 74–81. [[CrossRef](#)] [[PubMed](#)]
38. Krust, D.; Gusbeth, C.; Müller, A.S.K.; Scherer, D.; Müller, G.; Frey, W.; Nick, P. Biological Signalling Supports Biotechnology–Pulsed Electric Fields Extract a Cell-Death Inducing Factor from *Chlorella Vulgaris*. *Bioelectrochemistry* **2022**, *143*, 107991. [[CrossRef](#)] [[PubMed](#)]
39. Canelli, G.; Kuster, I.; Jaquenod, L.; Buchmann, L.; Murciano Martínez, P.; Rohfritsch, Z.; Dionisi, F.; Bolten, C.J.; Nanni, P.; Mathys, A. Pulsed Electric Field Treatment Enhances Lipid Bioaccessibility While Preserving Oxidative Stability in *Chlorella Vulgaris*. *Innov. Food Sci. Emerg. Technol.* **2022**, *75*, 102897. [[CrossRef](#)]
40. Cao, Y.; Yang, S.; Wang, J.; Kong, W.; Guo, B.; Xi, Y.; Zhang, A.; Yue, B. Metabolomic Exploration of the Physiological Regulatory Mechanism of the Growth and Metabolism Characteristics of *Chlorella Vulgaris* under Photoautotrophic, Mixotrophic, and Heterotrophic Cultivation Conditions. *Biomass Bioenergy* **2023**, *173*, 106775. [[CrossRef](#)]
41. Kandušer, M.; Belič, A.; Čorović, S.; Škrjanc, I. Modular Serial Flow Through Device for Pulsed Electric Field Treatment of the Liquid Samples. *Sci. Rep.* **2017**, *7*, 8115. [[CrossRef](#)] [[PubMed](#)]
42. Fan, Y.; Yi, J.; Zhang, Y.; Yokoyama, W. Fabrication of Curcumin-Loaded Bovine Serum Albumin (BSA)-Dextran Nanoparticles and the Cellular Antioxidant Activity. *Food Chem.* **2018**, *239*, 1210–1218. [[CrossRef](#)]
43. Xia, W.; Zhu, L.; Delahaije, R.J.B.M.; Cheng, Z.; Zhou, X.; Sagis, L.M.C. Acid-Induced Gels from Soy and Whey Protein Thermally-Induced Mixed Aggregates: Rheology and Microstructure. *Food Hydrocoll.* **2022**, *125*, 107376. [[CrossRef](#)]
44. Subaşı, B.G.; Jahromi, M.; Casanova, F.; Capanoglu, E.; Ajalloueiian, F.; Mohammadifar, M.A. Effect of Moderate Electric Field on Structural and Thermo-Physical Properties of Sunflower Protein and Sodium Caseinate. *Innov. Food Sci. Emerg. Technol.* **2021**, *67*, 102593. [[CrossRef](#)]
45. Tian, Y.; Zhang, Z.; Zhang, P.; Taha, A.; Hu, H.; Pan, S. The Role of Conformational State of pH-Shifted β -Conglycinin on the Oil/Water Interfacial Properties and Emulsifying Capacities. *Food Hydrocoll.* **2020**, *108*, 105990. [[CrossRef](#)]
46. Zhao, F.; Liu, X.; Ding, X.; Dong, H.; Wang, W. Effects of High-Intensity Ultrasound Pretreatment on Structure, Properties, and Enzymolysis of Soy Protein Isolate. *Molecules* **2019**, *24*, 3637. [[CrossRef](#)] [[PubMed](#)]
47. Tong, X.; Cao, J.; Tian, T.; Lyu, B.; Miao, L.; Lian, Z.; Cui, W.; Liu, S.; Wang, H.; Jiang, L. Changes in Structure, Rheological Property and Antioxidant Activity of Soy Protein Isolate Fibrils by Ultrasound Pretreatment and EGCG. *Food Hydrocoll.* **2022**, *122*, 107084. [[CrossRef](#)]
48. Wang, H.; Wang, N.; Chen, X.; Wu, Z.; Zhong, W.; Yu, D.; Zhang, H. Effects of Moderate Electric Field on the Structural Properties and Aggregation Characteristics of Soybean Protein Isolate. *Food Hydrocoll.* **2022**, *133*, 107911. [[CrossRef](#)]

Disclaimer/Publisher’s Note: The statements, opinions and data contained in all publications are solely those of the individual author(s) and contributor(s) and not of MDPI and/or the editor(s). MDPI and/or the editor(s) disclaim responsibility for any injury to people or property resulting from any ideas, methods, instructions or products referred to in the content.